Cheung, R., Castrichini, A., Rezgui, D., Cooper, J., & Wilson, T. (2018). Wind Tunnel Testing of Folding Wing-Tip Devices for Gust Loads Alleviation. In *17th International Forum on Aeroelasticity and Structural Dynamics (IFASD 2017): Proceedings of a meeting held 25-28 June 2017, Como, Italy* (pp. 534-550). [IFASD-2017-049]

WIND TUNNEL TESTING OF FOLDING WING-TIP DEVICES FOR GUST LOADS ALLEVIATION

R.C.M. Cheung[1], A. Castrichini[1], D. Rezgui[1], J.E. Cooper[1] and T. Wilson[2]

[1] Department of Aerospace Engineering, University of Bristol
University Walk, Bristol, BS8 1TR, UK.
r.c.m.cheung@bristol.ac.uk

[2] Airbus Operations Ltd
Filton, Bristol, BS34 7PA, UK.
thomas.wilson@airbus.com

Keywords: folding wing-tip, gust loads alleviation, wind tunnel testing.

Abstract: An increasing number of recent aircraft designs have begun considering the use of higher aspect ratio wings for reducing induced drag to improve fuel consumption. The increased wing span has led to the introduction of folding wing-tips as a solution for meeting airport gate requirements. Recent numerical studies have suggested such folding wing-tip solutions may be incorporated with spring devices to provide gust loads alleviation in flight as well. A series of low-speed wind tunnel tests was conducted in order to demonstrate such a concept using a prototype model. It was found that gust loads alleviation could be achieved using a folding wing-tip with a non-zero relative angle of the folding hinge axis to the stream-wise direction. The best loads alleviation performance varied with hinge angle setting and hinge stiffness, as well as lifting condition.

NOMENCLATURE

α	= Angle of attack	k_θ	= Torsional spring stiffness
Λ	= Sweep angle	k_x	= Linear spring stiffness
θ	= Fold angle of the wing-tip	V	= Wind tunnel speed
γ	= Hinge angle		

1 INTRODUCTION

It is well known from the classic Breguet range equation that aircraft with more fuel-efficient engines, better aerodynamic lift-drag ratio or lower structural weight can fly further. Consequently, an aircraft with any of these attributes can cover the same distance carrying a higher payload or using less fuel. For airframe designers, this means targeting the aerodynamics and/or the structural weight. One simple approach for improving the aerodynamic performance is through increasing the aspect ratio of the wing, which decreases the associated induced drag. However, increasing the wing span increases structural weight, and so the trade-off between the improved aerodynamics and increased weight must be considered. A further factor is the operating difficulties that may occur as existing airport gates may be too narrow, and indeed, airlines are charged by the size of the gate that are used. Trying to achieve these two contrasting planform requirements, high aspect ratio in flight and low span on the ground, points towards

the wider field of morphing structures research [1-5], which in part focuses on changing the geometry of the aircraft during its operation. The field of morphing covers larger geometric [1] changes, including sweep and span, to finer shape changes such as camber and section thickness, which tend to be more focused on application of specific materials [6] or devices [7].

One of the simplest morphing solutions for variable span requirement is in the form of a folding wing-tip, which is soon to be deployed in the latest civil aircraft [8], as it can be achieved using conventional materials and mechanisms through a hinged design. The hinge mechanism allows the wing-tip to be folded up as the aircraft taxis to the gate, and is locked in its extended position before take-off. Morphing of the wing-tip has in fact received significant interest within the field itself as the wing-tip has been identified with great potentials to fulfil a wider goal of enabling optimized performance in varying conditions throughout the flight. The main benefit of wing-tip morphing is its relatively small size compared to the planform, yet it can have a large influence on wing root loading due to its considerable distance from the wing root itself as well as being aerodynamically important for stall, drag and manoeuvrability.

For gust loads alleviation, the large moment arm offered by the wing-tip for influencing the wing root bending moment has been the main reason for their selection in their respective studies, which include Miller [9, 10], Guo [11, 12] and Ricci [13] who considered a passive movable aerodynamic surface at the wing-tip. The device was connected to the main airframe through a torque tube in the span-wise direction, which provided additional torsional stiffness about a location forward of the wing-tip's centre of pressure. The device functioned by reacting to vertical gusts through nose-down deflection in a passive manner, which alleviated the load increment caused by the gusts in the process. Although good loads alleviation capability was observed, it had a detrimental effect on flutter, especially when low torsional stiffness torque tubes were used.

Another approach for gust loads alleviation is through a folding wing-tip device that has an offset hinge axis from the longitudinal axis of the aircraft. The idea for such a device originates from the observation that when the orientation of the axis of which folding of the wing-tip occurs is strongly linked to the effective geometric twist of the wing-tip as it folds, which is described by

$$\Delta\alpha = -\tan^{-1}(\tan\theta\sin\gamma) \tag{1}$$

where the orientation of the axis is expressed as a function of the hinge angle γ in Figure 1 and the fold angle θ in Figure 2.
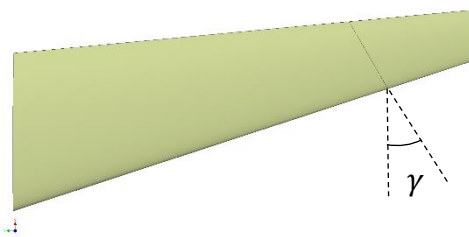

Figure 1: Planform view showing the hinge angle γ.

Figure 2: Front view showing the fold angle θ.

Consequently, the zero-angled hinge angle shown in Figure 3 provides no gust loads alleviation capability, whereas a positive hinge angle, as shown in Figure 4, can provide potential loads alleviation benefit during vertical gust encounters due to the decreased twist (local angle of attack) beyond the fold, as this action reduces the resulting bending moment contribution.

Figure 3: Front view showing positive fold angle for a hinge angle of 0^0.

Figure 4: Front view showing positive fold angle for a hinge angle of 30^0.

By exploiting this effect, a folding wing-tip has the potential to fulfil both the airport gate requirement, and to provide gust loads alleviation capability, by incorporating a non-zero hinge angle in its design. A number of numerical studies have been carried out to investigate the feasibility and performance of using a device of this type, in addition to a passive spring system at the hinge in order to control its dynamic behaviour and exploit the potential gust loads alleviation capability. A preliminary study [14] has found that a linear spring device can provide load-alleviating benefit when both the hinge stiffness and wing-tip inertia are low. However, low hinge stiffness can cause the wing-tip to remain in a deflected position even in a trimmed-flight condition, which has an undesirable effect on the overall aerodynamics. This differing optimal stiffness for trimmed-flight and gust loads alleviation has led to proposed solutions such as bi-stable wing-tips [15] and active control via piezoelectric actuators [16]. Despite this complication, the folding wing-tip concept remains promising as recent research have suggested that coupling the folding wing-tip to a nonlinear spring system may provide the solution [17, 18].

The work described in this paper aims to obtain baseline experimental data of the folding wing-tip concept when coupled with a linear spring device, particularly focusing on the effect of a non-zero hinge angle has on the its gust loads alleviation performance through low-speed wind tunnel testing. This is a continuation of the previous study by the authors [19], in which only a single hinge angle setting was experimentally investigated in a wind tunnel setting. The current work expands on the research through testing two hinge angle settings as well as taking advantage of utilising a better performing gust generator for testing the dynamic response of the folding wing-tip prototype.

2 WIND TUNNEL MODEL

2.1 Design

This investigation aims at establishing the effect of the hinge angle on the overall gust loads alleviation performance. Therefore, the span of the wind tunnel model has been maximised to the largest permissible semi-span for the working section at approximately 0.7m to allow more accurate bending moment measurement, since peak bending moment reduction is a prime measure of gust loads alleviation performance. The model has a constant symmetric NACA0015 section profile with chord of approximately 0.3m as shown in Figure 5 (a).
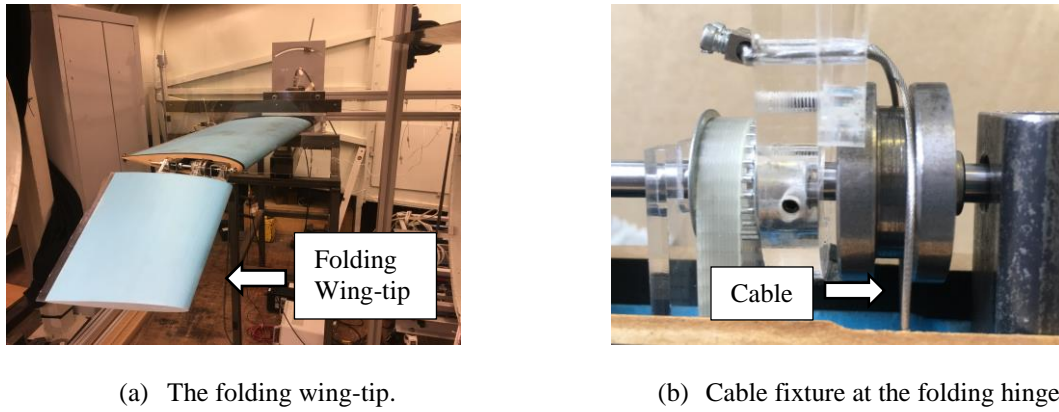
(a) The folding wing-tip.

(b) Cable fixture at the folding hinge.

Figure 5: Wind tunnel model.

The choice of a comparatively thick NACA0015 section was based on the need to increase the internal volume for the spring system, which requires a cable linkage from the hinge to the outside of the wind tunnel, enabling a range of different springs to be attached to the wing tip at the hinge. The choice of different springs is required as part of the investigation was focusing on the effect of hinge stiffness. The cable linkage functions through translating the angular displacement of the wing-tip into translational displacement of the cable, as shown in Figure 6, allowing the use of linear tension springs to represent a torsional spring fitted at the hinge. The equivalent torsional stiffness is given by

$$k_\theta = k_x \frac{dx}{d\theta} \tag{2}$$

As shown in Figure 5 (b), the fixture at the hinge has been designed so that the cables will always depart at the same direction and distance away from the hinge, thus ensuring the derivative in Equation (2) is constant and a linear mapping is retained. The dual cable design enables both cables to remain in tension at all fold angles through pre-tensioning, thus ensuring consistency in the spring tension provided by both springs.
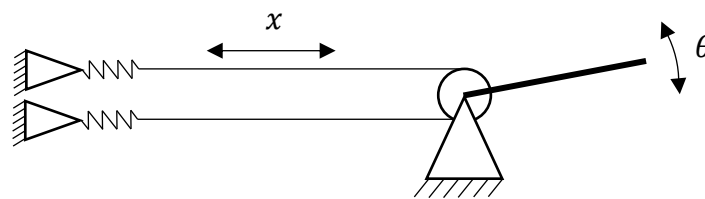

Figure 6: Schematic of the spring system.

The wind tunnel model has been designed with variable sweep while having the hinge axis fixed relative to the body of the model itself. The reason for this approach is to allow the effective hinge angle to be varied through a change in sweep angle, as well as keeping swapping of parts to a minimum. The orientation of the hinge axis is normal to the leading edge, which gives a simple mapping between the hinge angle and the sweep angle.

$$\gamma = \Lambda \tag{3}$$

4

As illustrated in Figure 7, the variable sweep design requires shielding from the airflow at the wing-root, therefore as the sweep angle is increased, the total exposed wing area and span are reduced. To compensate for these changes, a customised wing-tip is used at each test sweep angle. Each wing-tip is sized to approximately 25% of the total exposed wing area of its corresponding test configuration, and shaped such that the tip of the overall wing terminates in a consistent manner. Foam construction has been chosen to ease the manufacturing process, as well as minimising the inertia and mass of the wing-tips. In this wind tunnel test campaign, a total of two sweep configurations: 10° and 30° were prepared and tested.

| (a) Sweep angle of 10°. | (b) Sweep angle of 30°. |
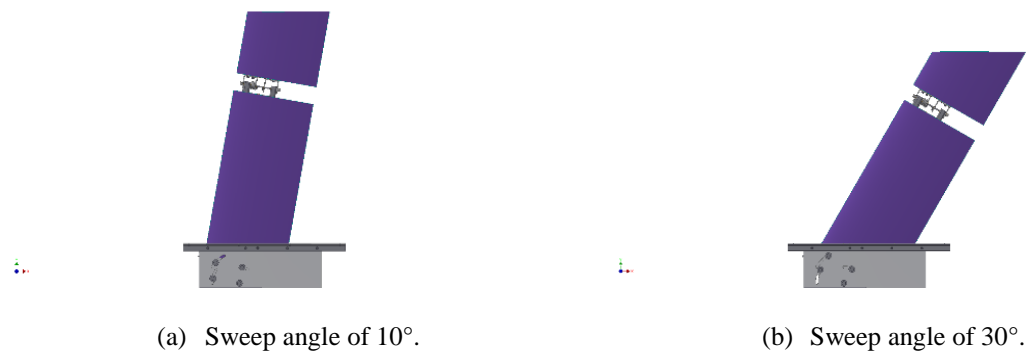
Figure 7: Variable sweep design.

2.2 Test set-up and instrumentation

The wind tunnel tests were carried out in the open-jet wind tunnel at the University of Bristol, as shown in Figure 8. The test campaign consisted of a set of steady aerodynamic tests and a set of dynamic tests through gust excitation. In each test, lift, rolling moment, fold angle and hinge moment at the folding hinge were recorded. For assessing gust loads alleviation performance, the rolling moment is the key measurement since it can be translated directly to the wing root bending moment that the aircraft may experience. The main body forces and moments were measured using a custom-built frame in combination of two AMTI MC3A force and torque sensors [20], while the fold angle was monitored using a RLS RE22 rotary magnetic shaft encoder [21]. The hinge moment was derived from the cable tension measured through two RDP Model 31 load cells [22]. Data acquisition was enabled using a National Instruments USB-6211 and LabVIEW software [23].

For the steady aerodynamic tests, a stiff-hinge and a free-hinge arrangement were used, while the dynamic tests additionally included a sprung-hinge arrangement. As illustrated in Figure 6, this sprung-hinge arrangement was set up using two linear springs, each with measured stiffness of 195N/m. This set-up gave an equivalent torsional stiffness of 0.043Nm/rad with the pulley radius at 10.5mm. The pre-load applied to these springs were such that the net hinge moment due to the springs was near zero at fold angle of 0°. The stiff-hinge arrangement was achieved by removing the springs and connecting the cables directly to the load cells, while the free-hinge arrangement was set up simply through disconnecting the cables from the wing-tip.

The dynamic tests additionally involved installing a gust vane, as pictured in Figure 9, ahead of the wind tunnel model to perturb the oncoming flow. The gust vane was actuated manually with a stop mechanism to ensure the flow excitation was consistent. At each test point, the gust vane was deflected upwards once to produce a single positive vertical gust.
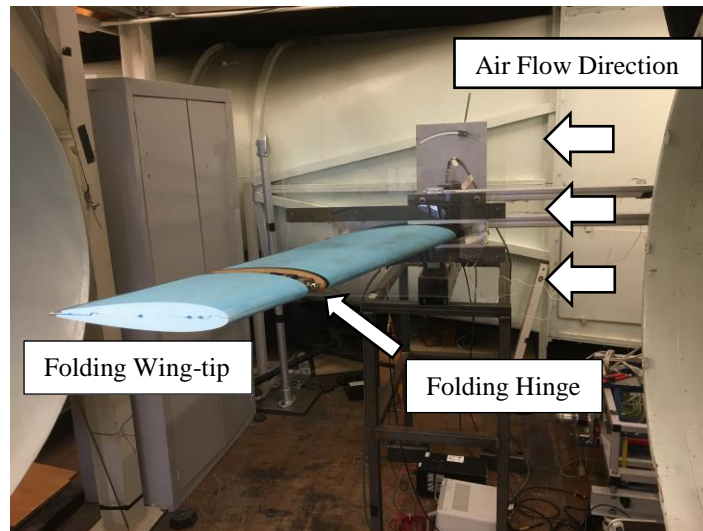
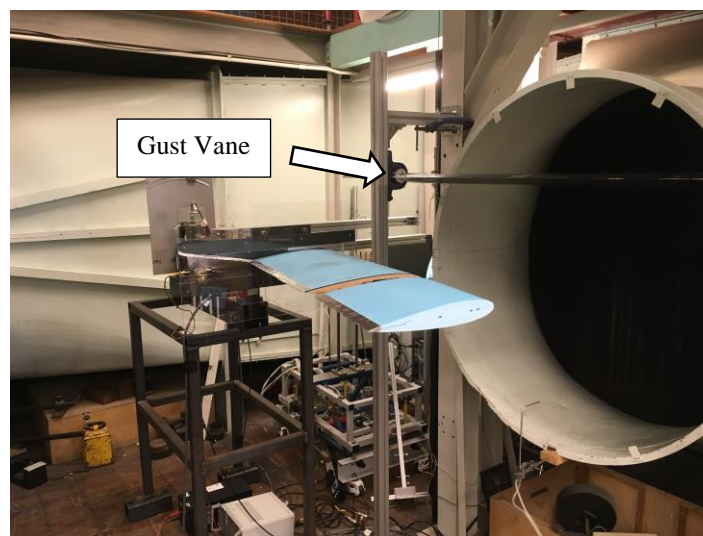Figure 8: Steady aerodynamic test setup.

Figure 9: Gust excitation setup.

3 RESULTS

The wind tunnel model was tested at its 10° and 30° hinge angle configuration, corresponding to a sweep angle of 10° and 30° respectively. For clarity and convenience, each configuration will be referred to the name given in Table 1 from hereon in.

Configuration	Sweep/hinge angle (°)	Reference chord (m)	Reference semi-span (m)
SWP10	10	0.305	0.856
SWP30	30	0.346	0.711

Table 1. Reference dimensions of the wind tunnel model configurations

3.1 Steady aerodynamics

In the steady aerodynamic test, the stiff-hinge and free-hinge configuration were examined; with angle of attack varying from -10° to 10° in increments of 5° and wind speed at 10, 12,

15, 18 and 20m/s. At every test point, the wing-tip settled to a steady fold angle once the flow had stabilised, demonstrating aerodynamic stability as expected.

As shown in Figure 10(a) and Figure 13(a), both hinge-angle configurations with the stiff-hinge arrangement showed linear lift-curves, as expected on of a non-folding wing-tip setup. With the free-hinge arrangement, the SWP10 configuration showed a mostly linear lift-curve except for a noticeable drop-off in lift towards high angle of attack in Figure 10(b). This reduction in lift was caused by the fold angle settling above zero, as shown in Figure 12(b), which lowered the lift generated at the wing-tip due the nose-down aerodynamic twist imposed by the hinge geometry at such fold angle. This effect is further highlighted by Figure 11(b), which shows the rolling moment was also reduced at higher lifting conditions.
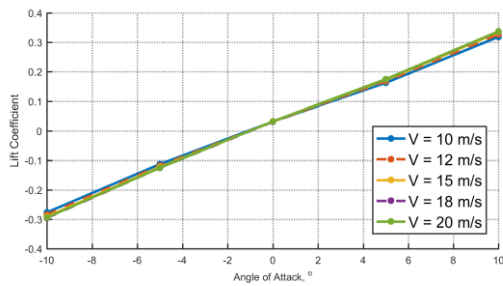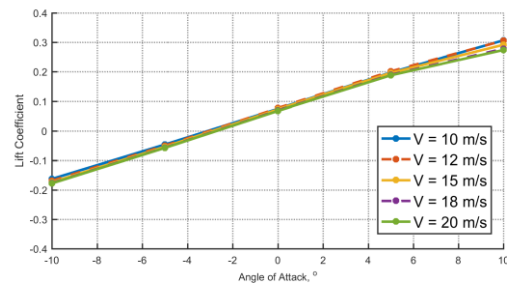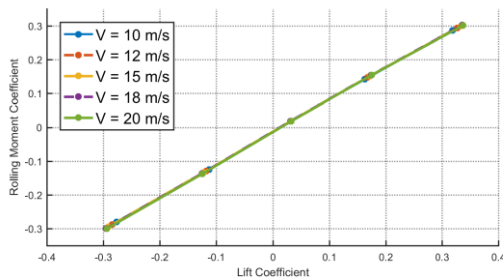

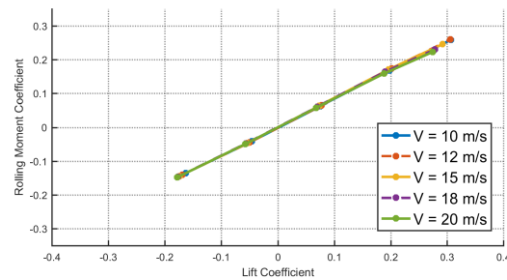(a) Stiff-hinge configuration.
(b) Free-hinge configuration.

Figure 10: Variation of measured lift coefficient with angle of attack for the SWP10 configuration.
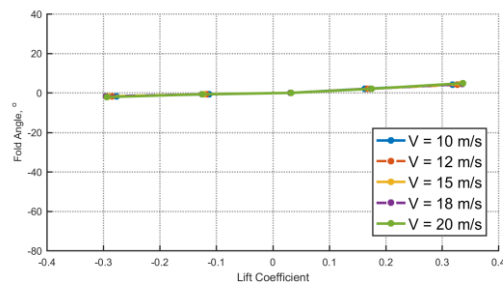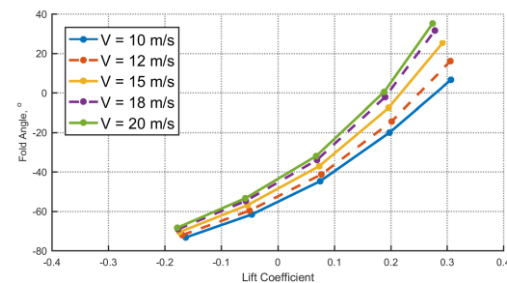

(a) Stiff-hinge configuration.
(b) Free-hinge configuration.

Figure 11: Variation of measured rolling moment coefficient against measured lift coefficient for the SWP10 configuration.
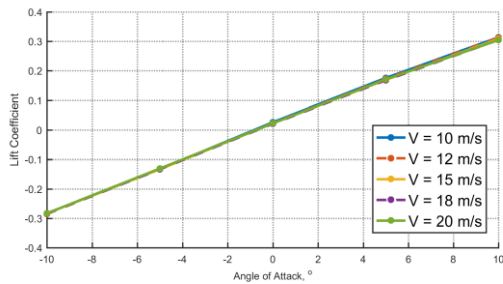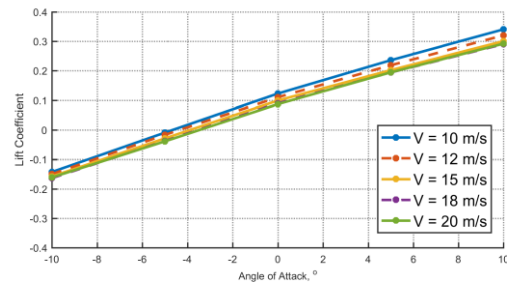

(a) Stiff-hinge configuration.
(b) Free-hinge configuration.

Figure 12: Variation of measured fold angle against measured lift coefficient for the SWP10 configuration.

For the SWP30 configuration with the free-hinge arrangement, as shown in Figure 13(b), the gentle reduction in lift-curve slop can be explained in similar manner through comparing the aero-static fold angle provided in Figure 15(b). In these cases, the fold angle was mostly in the negative region, therefore, wing-tip was in fact producing higher lift than at zero-fold. This also explains the more significant offset at zero angle of attack than the stiff-hinge case for this symmetric aerofoil-based wing. For the rolling moments, as shown in Figure 14(b), increasing wind tunnel speed shifted the curve downwards because less lift was generated at the wing-tip as the fold angle became more positive.
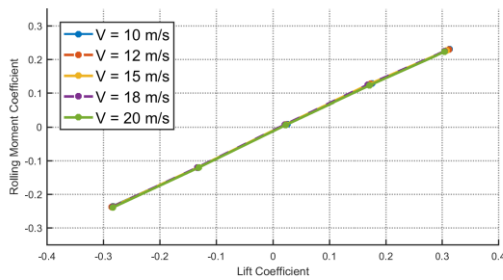

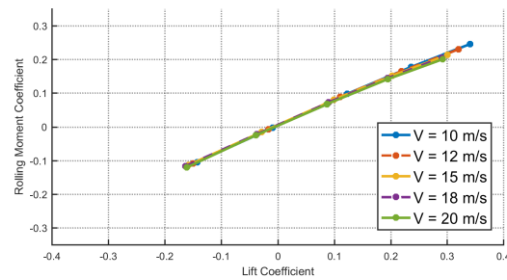(a) Stiff-hinge configuration.

(b) Free-hinge configuration.

Figure 13: Variation of measured lift coefficient with angle of attack for the SWP30 configuration.
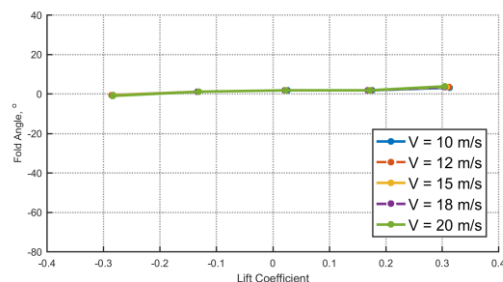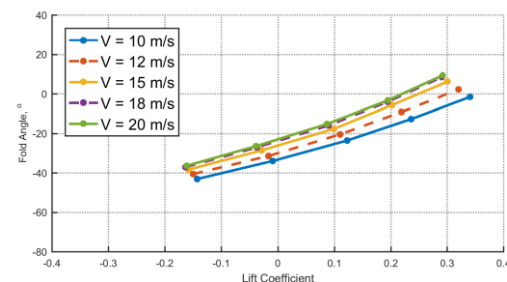

(a) Stiff-hinge configuration.

(b) Free-hinge configuration.

Figure 14: Variation of measured rolling moment coefficient against measured lift coefficient for the SWP30 configuration.

(a) Stiff-hinge configuration.

(b) Free-hinge configuration.

Figure 15: Variation of measured fold angle against measured lift coefficient for the SWP30 configuration.

In Figure 11 and Figure 14, the relationship between rolling moment and lift is linear for the stiff-hinge configuration in all three hinge-angle cases. There were no significant variations in the lift-curve across different speeds, which is consistent with a non-folding wing-tip configuration. In each case, the free-hinge configuration also demonstrates linearity but with

marginally steeper gradient at lower speeds. This behaviour is the result of the wing-tip reaching a more negative aero-static fold angle at these conditions, raising the rolling moment as larger amount of positive lift is generated at the wing-tip.

3.2 Comparison with numerical model

A set of numerical models has been constructed based on the Finite Element Method. The primary aim of this part of the work is to model the static and the dynamic behaviour of the folding wing-tip concept to help exploring the effect of changing design parameters. NASTRAN was used as the software package for this modelling work because calculating aeroelastic prediction through its in-built Doublet Lattice Method [24, 25] (DLM) implementation is already a widely adopted process within the aerospace industry.

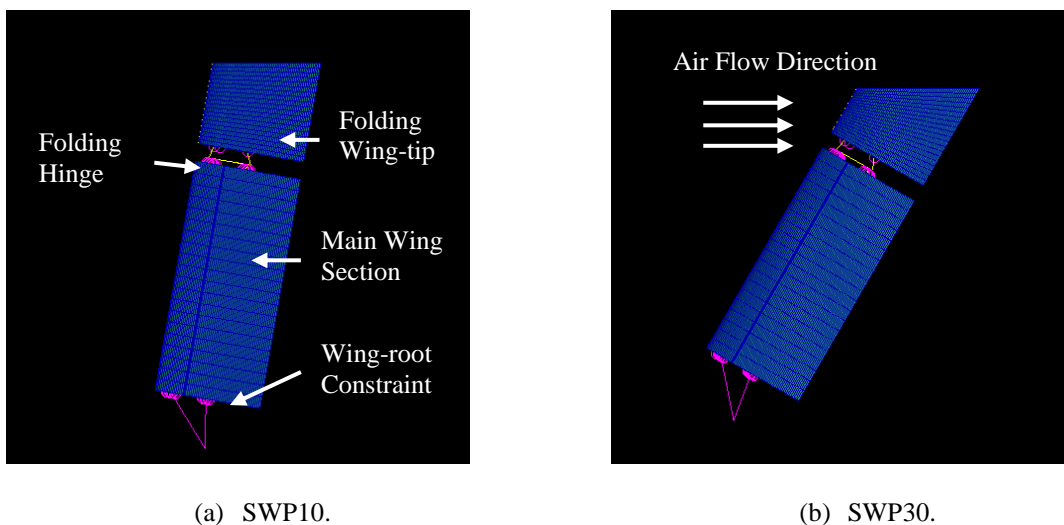(a) SWP10.   (b) SWP30.

Figure 16: Schematic representation of the FEMs used.

As shown in Figure 16, two Finite Element models (FEM) were constructed for this work. The necessity for constructing several FEMs originates from the geometric differences across the tested hinge angle configurations as laid out in Table 1. Efforts have been made to keep the number of elements in each model the same to preserve as much numerical consistency as possible.

Each model consists of a mixture of two-dimensional bar elements for the internal structure and three-dimensional elements for the external part of the wing. The hinge mechanism was modelled using a released rotational degree of freedom along the hinge axis, and the addition of a torsional spring elements of the appropriate stiffness attached in each hinge configuration.

The aerodynamic panels, which are needed for predicting the aerodynamic loads through the DLM, are shown in Figure 17 along with their relative position to the structural FEM. As shown in Figure 17(b), a triangular region around the inboard area of the wing-tip is deliberately ignored due to geometric limitation of DLM. Since all panels must align with the down-stream direction in DLM, constructing a panelled region there would imply the root side of the wing-tip is a leading edge. Although this is not strictly false, such an aerodynamic implication would be unrealistic as the real structure resembles closer to a bluff body due to its thickness rather than a flat plate that DLM is modelling. To compensate for this reduction in total panelled area, a scaling factor has been applied to the remaining wing-tip panels such that the total loads would be similar. The scaling is applied proportionally based on area ratio of the missing triangular

9

region and through changing the lift-curve correction factor (WKK in NASTRAN) for each applicable panel. It is important to note that DLM can only compute loads normal to the surface of each panel and an associated pitching moment due to the limitation of the potential flow theory it is based upon. Therefore, no drag can be computed with accuracy regardless of panel configuration, and even then, it is only the induced drag that is calculated.
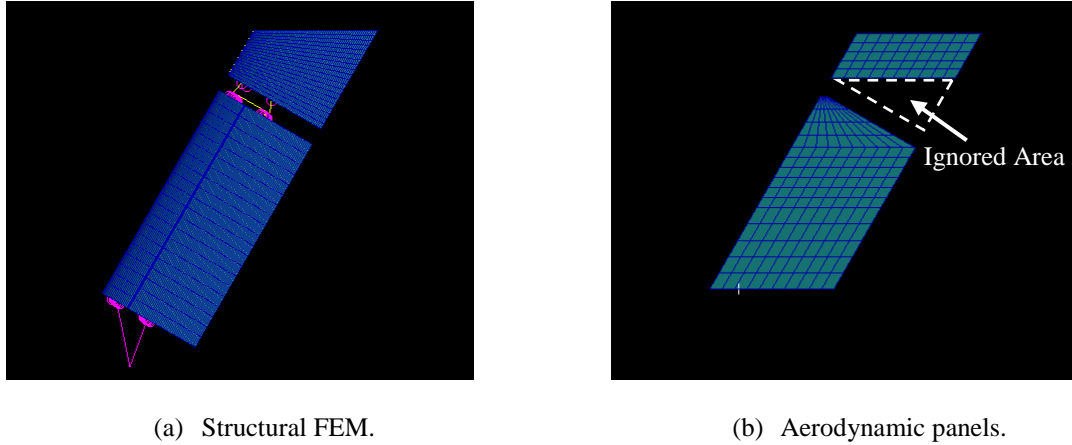

(a) Structural FEM.

(b) Aerodynamic panels.

Figure 17: Aeroelastic FEM.

(a) Hinge spring stiffness of K = 1E9Nm/rad, with filled markers showing wind tunnel measurements from the stiff-hinge configuration.

(b) Hinge spring stiffness of K = 1E-6Nm/rad, with filled markers showing wind tunnel measurements from the free-hinge configuration.
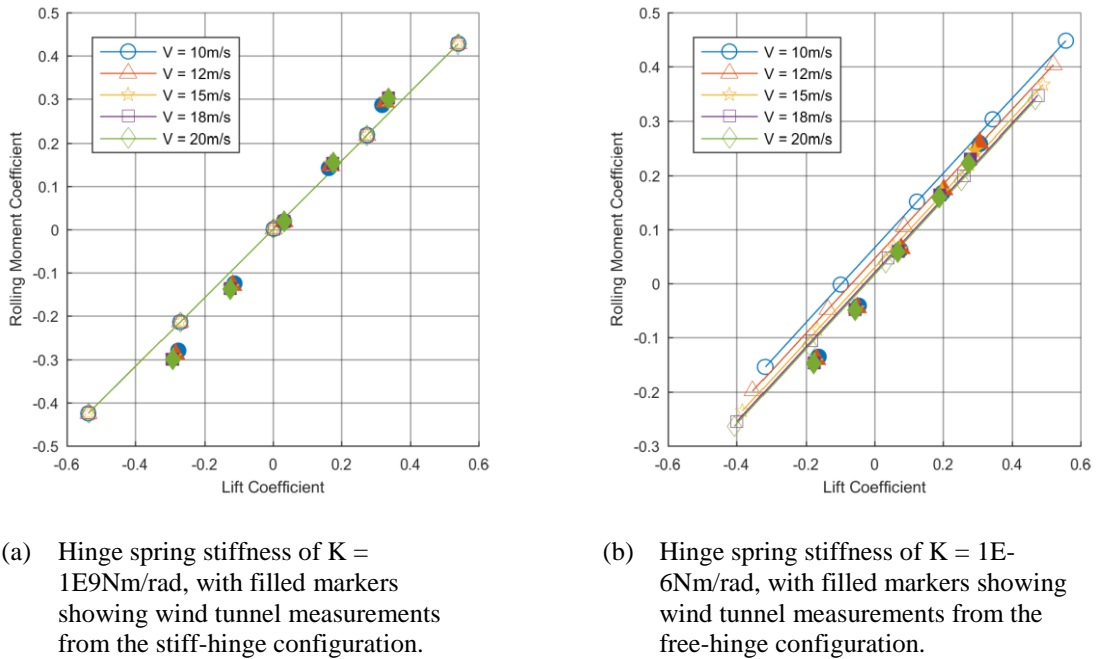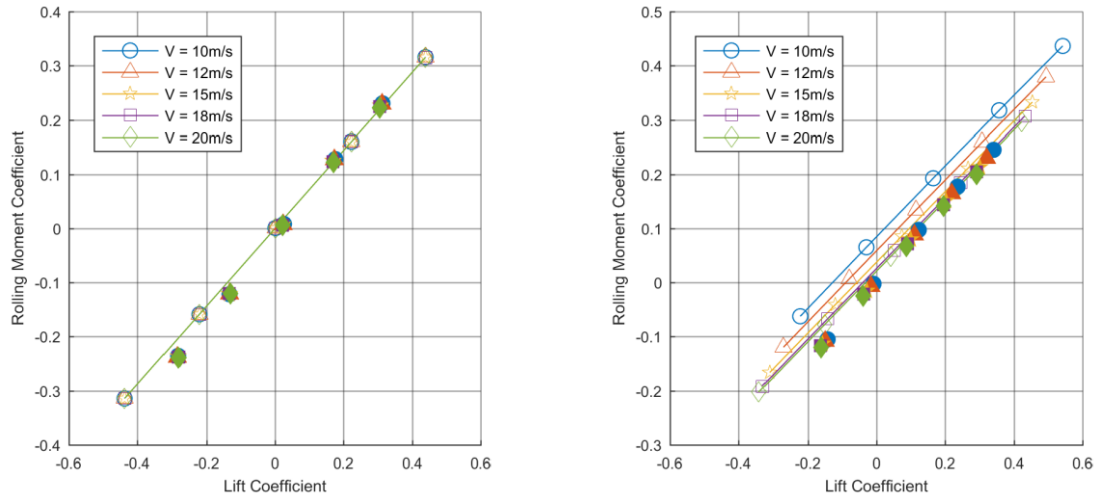
Figure 18: Variation of rolling moment coefficient against lift coefficient for SWP10 compared with wind tunnel measurements.

(a) Hinge spring stiffness of K = 1E9Nm/rad, with filled markers showing wind tunnel measurements from the stiff-hinge configuration.

(b) Hinge spring stiffness of K = 1E-6Nm/rad, with filled markers showing wind tunnel measurements from the free-hinge configuration.

Figure 19: Variation of rolling moment coefficient against lift coefficient for SWP30 compared with wind tunnel measurements.

Figure 18 and Figure 19 show the comparison between the wind tunnel test and FEM results for the SWP10 and the SWP30 configuration respectively. The stiff-hinge arrangement corresponds to the highest spring stiffness case of K = 1E9Nm/rad in the FEM, while the free-hinge arrangement is matched with the lowest stiffness case of K = 1E-6Nm/rad. The low stiffness case is the best approximation to the free-hinge arrangement because NASTRAN cannot produce reliable results when a mechanism is present in the FEM (i.e. K = 0Nm/rad).

Both the SWP10 and the SWP30 configuration show good correlation with the wind tunnel test data for both hinge arrangments. However, the wind tunnel data generally shows a higher bending moment coefficient for a given lift coefficient. This difference is attributed by the characteristic of the wind tunnel setup in which the root region was at the boundary of the wind tunnel jet, resulting in lower overall lift generation. Despite this, the loss of lift near the wing root region meant the overall measured bending moment would be affected to a lesser extent due to a short moment arm. One of the key observations is that the agreement between the experimental and computational results are better at higher lift coefficients from 0.0 to 0.2 because the fold angle is nearing zero in these conditions for the SWP10 configuration and likewise lift coefficients around 0.2 to 0.4 for the SWP30 configuration. This behaviour limits the errors due to geometric nonlinearity within the linear analysis used by NASTRAN. Despite this inherent limitation, the FEMs produced a good agreement with the wind tunnel tests across the tested range of conditions, suggesting their usage for modelling this folding wing-tip concept for aero-static predictions is suitable.

3.3 Gust excitation

The SWP10 and the SWP30 configuration were tested at wind tunnel speed of 20m/s, with angle of attack varying from -10° to 10° in increments of 5°. Stiff-hinge, sprung-hinge and free-hinge arrangements were also tested along with each hing angle configuration. At each test point, the wind tunnel model was subjected to an upward gust excitation through deflection of the gust vane to a maximum of 10.0° from its neutral position.

(a) Lift coefficient.
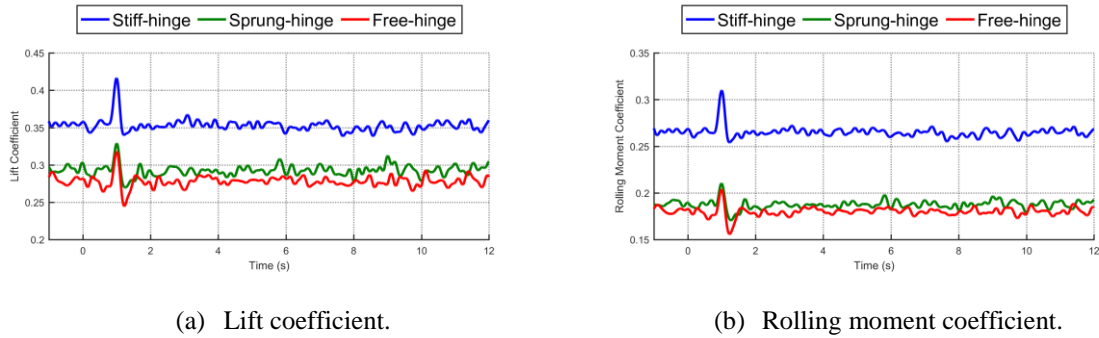
(b) Rolling moment coefficient.

Figure 20: Gust response of the SWP10 configuration at 10° angle of attack and wind speed of 20m/s.

Figure 20 shows a typical response in lift and rolling moment during gust excitation, while Figure 22 and Figure 23 show the upper and lower bound of the dynamic load envelope. These values have been calculated using the definitions outlined in Figure 21 to determine the upper and the lower bound based on the difference between the maximum and the minimum from the mean steady state respectively.
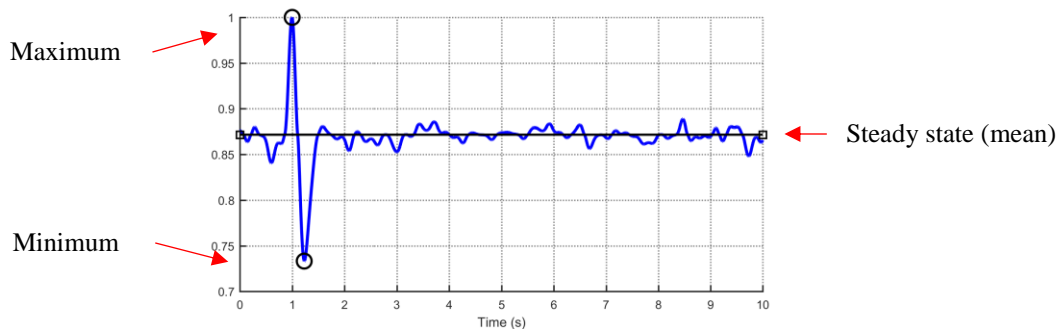

Figure 21: Terminology and their definitions in the context of the dynamic measurements.

From Figure 22(c) and (f), both the upper and lower bound of the fold angle response for the stiff-hinge arrangement were small, demonstrating the suitability of using the stiff-hinge data as the non-folding wing-tip baseline for the SWP10 configuration. Similarly, the stiff-hinge arrangement for the SWP30 configuration was also set up correctly, basing upon the results shown in Figure 23(c) and (f).

In Figure 22(a), both the sprung-hinge and the free-hinge arrangement for the SWP10 configuration produced a lower peak change in lift across both positive and negative lifting conditions when compared with the stiff-hinge case. The free-hinge case generally had a smaller peak lift loading and the peak rolling moments were also lower as shown in Figure 22(b). This suggests the free-hinge arrangement is more effective in resolving the main issue in positive vertical gust encounters, where the peak wing-root bending moment increment may become critical for structural integrity. For the lower bound in rolling moment change, as shown in Figure 22(e), both the sprung-hinge and the free-hinge arrangement performed similarly to the stiff-hinge arrangement, except at the highest lifting case with lift coefficient of 0.3. In fact, both the sprung-hinge and the free-hinge arrangement had a sudden increase in magnitude of the rolling moment change from the previously lower lifting conditions. This also coincides with a smaller lower bound in fold angle change as shown in Figure 22(f). As seen from the steady aerodynamic test cases, a more negative fold angle produces higher positive lift at the wing-tip and more positive rolling moment is generated as a result. Therefore, the previously

12

lower lifting cases were in fact benefiting from this additional rolling moment for reducing the size of the lower bound. This sudden loss of negative rolling moment alleviation at lift coefficient of 0.3 may be attributed by the highly positive aero-static fold angle of approximately 38° in this condition, as shown in Figure 12(b), which means the wing-tip could not build up sufficient momentum to swing through to a more negative fold angle during its downwards motion as the assistance from the hinge moment due to the wing-tip weight diminishes at high fold angle.

(a) Upper bound of change in lift coefficient.

(b) Upper bound of change in rolling moment coefficient.

(c) Upper bound of change in fold angle.

(d) Lower bound of change in lift coefficient.

(e) Lower bound of change in rolling moment coefficient.
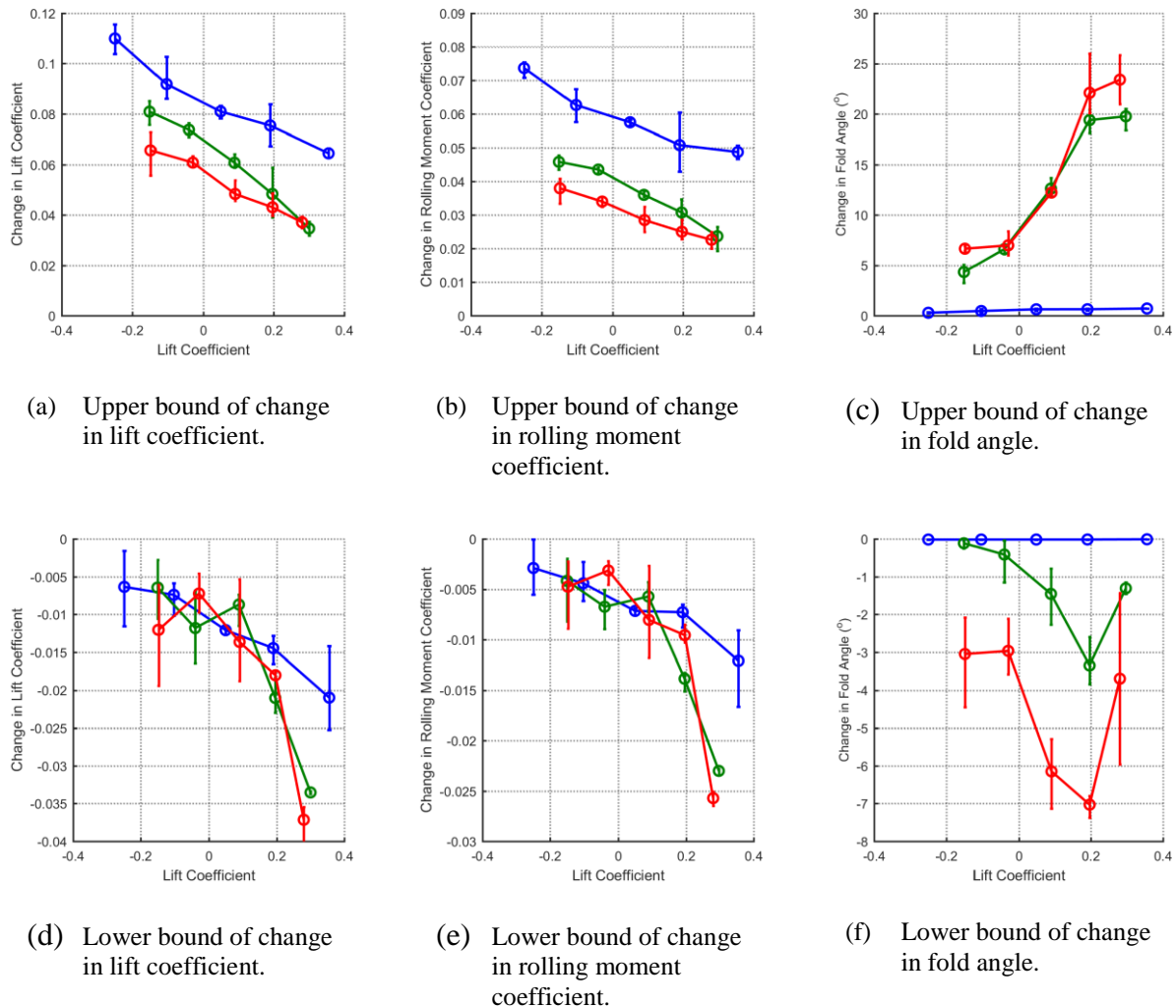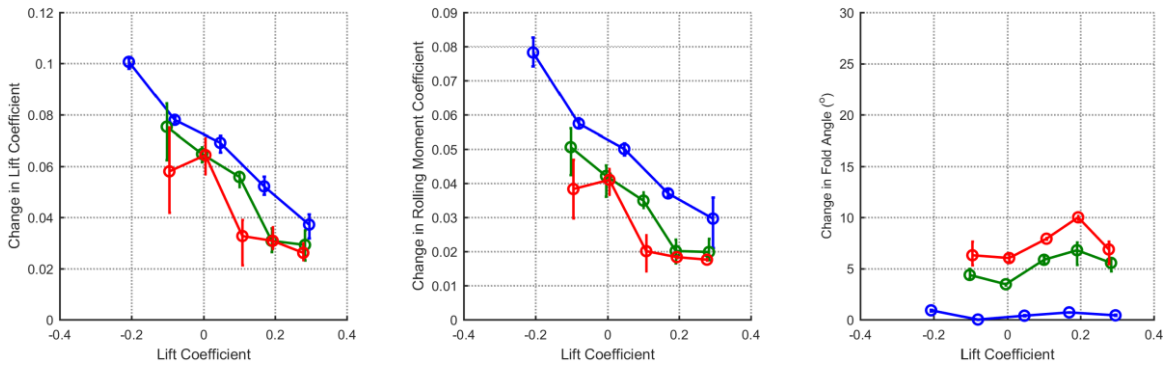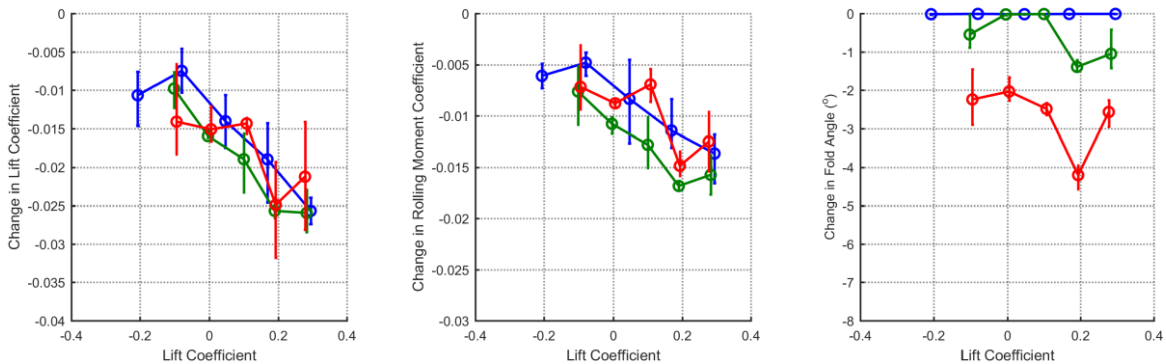
(f) Lower bound of change in fold angle.

Figure 22: Gust response of the SWP10 configuration at wind tunnel speed of 20m/s (see Figure 24 for plot legend).

For the SWP30 configuration, the general trend in gust loads alleviation is the same as the SWP10 configuration as shown by the lower peak loads in the sprung-hinge and the free-hinge arrangement in Figure 23(c) and (f). The free-hinge arrangement performed better than the sprung-hinge arrangement in terms of upper bounds, however marginal improvement is also observed in the lower bounds. Although the general trend in the lower bound in fold angle change follows the equivalent for the SWP10 configuration, as shown in Figure 23(f), the sudden increase in lower bound loads at higher lifting conditions was absent. This is consistent with the observation above as the SWP30 configuration had a generally less positive aero-static fold angle when compared with the SWP10 configuration. In terms of the fold angle upper bounds, the magnitude for the SWP30 configuration was smaller than the SWP10 configuration, as shown in Figure 22(c) and Figure 23(c). This effect is a direct result of utilising

a higher hinge angle because a larger, but more negative effective twist is applied to the wing-tip as it folds, meaning more negative lift is generated during the upwards motion of the wing-tip and decelerates the wing-tip more quickly before it can reach a higher fold angle.

(a) Upper bound of change in lift coefficient.

(b) Upper bound of change in rolling moment coefficient.

(c) Upper bound of change in fold angle.

(d) Lower bound of change in lift coefficient.

(e) Lower bound of change in rolling moment coefficient.

(f) Lower bound of change in fold angle.

Figure 23: Gust response of the SWP30 configuration at wind tunnel speed of 20m/s (see Figure 24 for plot legend).
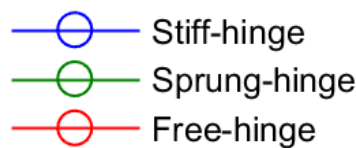

Figure 24: Plot legend for Figure 22 and Figure 23.

From Figure 22(b) and Figure 23(b), the best peak rolling moment reduction in each hinge angle configuration were both approximately 56% with the free-hinge arrangement in operation. For the SWP10 configuration, it occurred at lift coefficient of 0.3 while it was achieved at lift coefficient of 0.1 for the SWP30 configuration. The aero-static fold angle in this case was approximately -20° for the SWP30 configuration, as shown in Figure 15(b), which suggests good gust loads alleviation performance is still possible with a negative aero-static fold angle, if its magnitude is not excessively large.

4 CONCLUSIONS

A series of low-speed wind tunnel tests has been conducted on a folding wing-tip prototype with hinge angle set to 10° and 30°. A set of steady aerodynamic tests was carried out to examine the aero-static behaviour of the wing-tip against variation in hinge stiffness, and similarly for its dynamic response through gust excitations.

In the steady aerodynamic tests, the folding wing-tip was found to be statically aerodynamically stable with both the stiff-hinge and the free-hinge arrangement, and for both 10° and the 30° hinge angle settings, demonstrating inherent aerodynamic stability regardless of hinge stiffness. The free-hinge cases showed shallower overall lift-curves and lower rolling moment with increasing airspeed. This effect is the direct result of the positive hinge angle inducing lower aerodynamic twist on the wing-tip and lowering lift generation as it folds.

The steady measurements have also been compared with aeroelastic predictions generated using NASTRAN Finite Element models and found to be in good agreement. This finding suggests using a linear Finite Element Method with Doublet Lattice Method is suitable for modelling the aero-static behaviour of the folding wing-tip concept.

The gust excitation tests were also conducted using the 10° and the 30° hinge angle configuration. In both configurations, it was found that the free-hinge arrangement, and the sprung-hinge arrangement of intermediate added hinge stiffness, provided significant reduction in peak increase in rolling moment during gust excitations, thus demonstrating gust loads alleviation capability. In particular, using the free-hinge arrangement appeared to marginally outperform the sprung-hinge with the best case reaching a 56% reduction in peak rolling moment when compared with the stiff-hinge baseline.

5 ACKNOWLEDGMENTS

6 REFERENCES

[1] Livne E., Weisshaar T.A., Aeroelasticity of nonconventional airplane configurations-past and future, *Journal of Aircraft*, 40(6), pp.1047-1065, 2003.

[2] Friswell M.I., The prospects for morphing aircraft, in Smart Structures and Materials (SMART09), IV ECCOMAS Thematic Conference (pp. 175-188), 2009.

[3] Sofla A.Y.N., Meguid S.A., Tan K.T., Yeo W.K., Shape morphing of aircraft wing: status and challenges, *Materials & Design*, 1(3), pp.1284-1292, 2010.

[4] Barbarino S., Bilgen O., Ajaj R.M., Friswell M.I., Inman D.J., A review of morphing aircraft. *Journal of Intelligent Material Systems and Structures*, 22(9), pp.823-877, 2011.

[5] Ajaj R.M., Beaverstock C.S., Friswell M.I., Morphing aircraft: the need for a new design philosophy, *Aerospace Science and Technology*, 49, pp.154-166, 2016.

[6] Sun J., Guan Q., Liu Y., Leng J., Morphing aircraft based on smart materials and structures: A state-of-the-art review, *Journal of Intelligent Material Systems and Structures*, p.1045389X16629569, 2016.

[7] Cooper J.E., Chekkal I., Cheung R.C.M., Wales C., Allen N.J., Lawson S., Peace A.J., Cook R., Standen P., Hancock S.D., Carossa G.M., Design of a Morphing Wingtip, *Journal of Aircraft*, 52(5), pp.1394-1403, 2015.

[8]   Smith M.H., Renzelmann M.E., Marx A.D., The Boeing Company, 1995. *Folding wingtip system*. U.S. Patent 5,381,986.

[9]   Miller S., Vio G.A., Cooper J.E., Sensburg O., Optimisation of a scaled sensorcraft model with passive gust alleviation, in Proceedings of the 12th AIAA/ISSMO Multidisciplinary Analysis and Optimization Conference, MAO, Victoria, BC, Canada (Vol. 1012), 2008.

[10] Miller S., Vio G.A., Cooper J.E., Development of an Adaptive Wing Tip Device, 50th AIAA/ASME/ASCE/AHS/ASC Structures, Structural Dynamics, and Materials Conference, 2009.

[11] Guo S., Fu Q., Sensburg O.K., Optimal design of a passive gust alleviation device for a flying wing aircraft, in Proceedings of the 12th AIAA ATIO/14th AIAA/ISSMO MAO Conference, Session MAO-25, Indianapolis, IN, USA (Vol. 1719), 2012.

[12] Guo S., Los Monteros D., Espinosa J., Liu Y., Gust Alleviation of a Large Aircraft with a Passive Twist Wingtip, *Aerospace*, 2(2), pp.135-154, 2015.

[13] Ricci S., Castellani M., Romanelli G., Multi-fidelity design of aeroelastic wing tip devices, Proceedings of the Institution of Mechanical Engineers, Part G: *Journal of Aerospace Engineering*, p.0954410012459603, 2012.

[14] Castrichini A., Hodigere Siddaramaiah. V., Calderon. D.E., Cooper J.E., Wilson T. & Lemmens Y., "Preliminary Investigation of Use of Flexible Folding Wing-Tips for Static and Dynamic Loads Alleviation", *Aeronautical Journal,* Vol. 121, Issue 1235 January 2017, pp. 73-94.

[15] Gatto A., Mattioni F. and Friswell M. I., "Experimental Investigation of Bistable Winglets to Enhance Aircraft Wing Lift Takeoff Capability", *Journal of Aircraft*, Vol. 46, No. 2 (2009), pp. 647-655.

[16] Arrieta A. F., Bilgen O., Friswell M. I., Hagedorn P., "Dynamic control for morphing of bi-stable composites", *Journal of Intelligent Material Systems and Structures*, 24(3) 266–273.

[17] Castrichini A., Hodigere Siddaramaiah. V., Calderon. D.E., Cooper J.E., Wilson T. & Lemmens Y., "Nonlinear Folding Wing-Tips for Gust Loads Alleviation", *Journal of Aircraft* · February 2016, DOI: 10.2514/1.C033474.

[18] Castrichini A., Cooper J.E., Wilson T., A. Carrella & Lemmens Y., "Nonlinear Negative Stiffness Wing-Tip Spring Device for Gust Loads Alleviation", in *Journal of Aircraft* · November 2016, DOI: 10.2514/1.C033887.

[19] Cheung, R. C. M., Castrichini A., Rezgui D., Cooper J.E. and Wilson T., "Testing of Wing-Tip Spring Device for Gust Loads Alleviation." In 58th AIAA/ASCE/AHS/ASC Structures, Structural Dynamics, and Materials Conference, p. 0630. 2017.

[20] http://www.amti.uk.com/, retrieved 30 May 2017

[21] http://www.rls.si/, retrieved 30 May 2017

[22] http://www.rdpe.com/uk/men-load.htm, retrieved 30 May 2017

[23] http://www.ni.com/en-gb.html, retrieved 30 May 2017

[24] Albano E., Rodden W.P., A doublet-lattice method for calculating lift distributions on oscillating surfaces in subsonic flows. *AIAA journal*, 7(2), pp.279-285, 1969.

[25] Rodden W.P., Johnson E.H., *MSC/NASTRAN Aeroelastic Analysis Users Guide*, MSC Software, USA, 1994.

COPYRIGHT STATEMENT